1999-12-27

Aerosol dynamics in ship tracks

Russell, Lynn M.

Aerosol dynamics in ship tracks

Lynn M. Russell,[1] John H. Seinfeld,[2] Richard C. Flagan,[2] Ronald J. Ferek,[3]
Dean A. Hegg,[4] Peter V. Hobbs,[4] Wolfram Wobrock,[5] Andrea I. Flossmann,[5]
Colin D. O'Dowd,[6] Kurt E. Nielsen,[7] and Phillip A. Durkee[7]

Abstract. Ship tracks are a natural laboratory to isolate the effect of anthropogenic aerosol emissions on cloud properties. The Monterey Area Ship Tracks (MAST) experiment in the Pacific Ocean west of Monterey, California, in June 1994, provides an unprecedented data set for evaluating our understanding of the formation and persistence of the anomalous cloud features that characterize ship tracks. The data set includes conditions in which the marine boundary layer is both clean and continentally influenced. Two case studies during the MAST experiment are examined with a detailed aerosol microphysical model that considers an external mixture of independent particle populations. The model allows tracking individual particles through condensational and coagulational growth to identify the source of cloud condensation nuclei (CCN). In addition, a cloud microphysics model was employed to study specific effects of precipitation. Predictions and observations reveal important differences between clean (particle concentrations below 150 cm^{-3}) and continentally influenced (particle concentrations above 400 cm^{-3}) background conditions: in the continentally influenced conditions there is a smaller change in the cloud effective radius, drop number and liquid water content in the ship track relative to the background than in the clean marine case. Predictions of changes in cloud droplet number concentrations and effective radii are consistent with observations although there is significant uncertainty in the absolute concentrations due to a lack of measurements of the plume dilution. Gas-to-particle conversion of sulfur species produced by the combustion of ship fuel is predicted to be important in supplying soluble aerosol mass to combustion-generated particles, so as to render them available as CCN. Studies of the impact of these changes on the cloud's potential to precipitate concluded that more complex dynamical processes must be represented to allow sufficiently long drop activations for drizzle droplets to form.

1. Introduction

Ship-generated anomalous lines in marine stratiform cloud structures, visible in satellite imagery and commonly referred to as ship tracks, provide an opportunity to study cloud processing, including both marine boundary layer chemistry and interactions between anthropogenic aerosols and marine clouds. During the June 1994 Monterey Area Ship Track (MAST) experiment, off the coast of Monterey, California, the effect of ship exhaust was observed under continentally influenced and typical background marine conditions, with aerosol and cloud droplet measurements being made within the boundary layer, in the cloud layer, and in the free troposphere [Durkee et al., 2000a].

The goal of the present study is a comprehensive examination of the evolution of ship emissions in the marine boundary layer. We compare observations of the chemical and microphysical characteristics of ship emissions as functions of time since release with predictions of aerosol modification by condensation (in and below cloud), coagulation, and homogeneous/heterogeneous nucleation. This analysis provides a theoretical basis for understanding the processes important in the formation of ship tracks. We investigate the role of aerosols from several marine boundary layer sources, including sea spray, biogenic sulfur, and ship stack combustion prod-

[1] Department of Chemical Engineering, Princeton University, Princeton, New Jersey.

[2] Department of Chemical Engineering, California Institute of Technology, Pasadena, California.

[3] Office of Naval Research, Arlington, Virginia.

[4] Department of Atmospheric Sciences, University of Washington, Seattle, Washington.

[5] Department of Atmospheric Physics, Universite Blaise Pascale, Clermont-Ferrand, France.

[6] University of Sunderland, School of the Environment, Center for Marine and Atmopsheric Sciences, Durham, England.

[7] Department of Meteorology, Naval Postgraduate School, Monterey, California.

ucts. The ability of different particle populations to serve as sites for cloud droplet activation provides a basis for estimating the impact of anthropogenic aerosols on marine stratocumulus.

2. Ship Track Evolution

In the cloudy marine boundary layer, aerosols may grow by gas-to-particle conversion both below and in cloud, may activate to droplets in cloud, may coagulate with each other below cloud and with droplets in cloud, and may coalesce while activated in cloud. Sources of additional particles are those entrained from the free troposphere and from adjacent air masses. These processes control aerosol evolution for both natural and anthropogenic particles in the atmosphere.

Marine stratus clouds form when aerosol particles in moist air are activated, and this air is supersaturated by cooling as it is lifted to the top of the boundary layer. The activation of particles (of, e.g., 0.2 μm diameter) to cloud droplets (exceeding 10 μm diameter) increases particle surface area and collision cross section by several orders of magnitude.

Anthropogenic aerosol particles can provide additional potential cloud condensation nuclei (CCN) beyond those naturally present. If the anthropogenic particles are sufficiently large and hygroscopic to activate at the peak supersaturation reached in the updrafts forming the cloud, then the number of particles activated in supersaturated conditions increases over that under conditions without anthropogenic influence. However, since the number of particles activated and the maximum supersaturation attained in cloud are intrinsically dependent, both must be calculated simultaneously. The consequence of activating more particles is that water is removed from the vapor phase more quickly, such that given a constant rate of cooling in the air parcel, there is no longer as much "excess" water in the vapor phase, leading to a lower maximum supersaturation.

The structure of updrafts and downdrafts within clouds varies greatly with significant vertical and horizontal variations [Stevens et al., 1996]. Predicting these structures and the magnitude of the associated lapse rates is important for following the track evolution over the timescales of hours to days but would require a large eddy simulation (LES) approach. However, there is not yet a LES algorithm available which describes external mixtures of particles, forcing a choice of either accurate dynamics with simplified aerosol populations or detailed aerosol descriptions with simplified boundary layer circulation. In this study we use the latter approach to focus on the role of aerosol particle concentration, size distribution, and composition on cloud droplet activation and subsequent dynamics, using measured lapse rates and prescribed updraft velocities as fixed constraints in one-dimensional thermodynamic profiles.

In a uniform, stable stratus cloud layer, aerosol particles in parcels of air may be cycled repeatedly through cloud, undergoing successive cooling in updrafts and heating in downdrafts [Russell et al., 1994]. Ship tracks frequently persist for multiple days allowing time for numerous cycles of a single air parcel through cloud [Durkee et al., 2000b]. Ship track formation results in changes to the air parcel particle size distribution, which will affect the fraction of particles activating in subsequent updrafts. By predicting the relative rates of number and size change due to gas-to-particle conversion, coagulation, and cloud-processing, one may study how particles grow as the ship track evolves. Both the magnitude of the peak supersaturation in each successive cloud cycle and the presence of other particles that compete for water vapor will control the CCN available for droplet formation and associated cloud processing growth [Kaufman and Tanré, 1994]. Since this variation in supersaturation cannot be measured with current instrumentation, LES predictions are required to determine the impact of this spatial and temporal variability.

3. Aerosol Dynamics Model

To understand aerosol growth and activation processes and subsequent cloud droplet dynamics, we have constructed a numerical model and used it to evaluate data measured in the atmosphere [Russell and Seinfeld, 1998]. The impact of anthropogenic aerosol has been studied using three distinct aerosol populations in an externally mixed, fixed-sectional model of the nucleation, condensation, coagulation, and deposition processes of the aerosol. Growth and evaporation of particles during cloud formation are calculated by explicit accounting of wet and dry particle size to retain the separate compositions of activated particles.

The aerosol dynamics model is based on a fixed-sectional approach to representing the size domain, with internally mixed chemical components and externally mixed types of particles [Russell and Seinfeld, 1998]. By allowing a fixed set of species to condense onto any one of several predefined aerosol populations, the model allows each population to be described by a different internal mixture of species at a different size. Coagulation would tend to define increasing numbers of types of new "populations" resulting from combinations of existing populations, but to maintain a manageable number of aerosol types, we have used here a categorization based on the experimentally measurable quantity of particle volatility [Jennings and O'Dowd, 1990], in which particles of different populations that coagulate are assigned to the population with the least volatile components. Alternative schemes can be tailored to track specific chemical components, but this scheme also provides an optically important characterization of the mixture since those particles with involatile black carbon cores are the same particles that have insoluble, absorbing components. This algorithm provides a solution which retains some information about the degree of external mixing in a population although it necessarily lumps
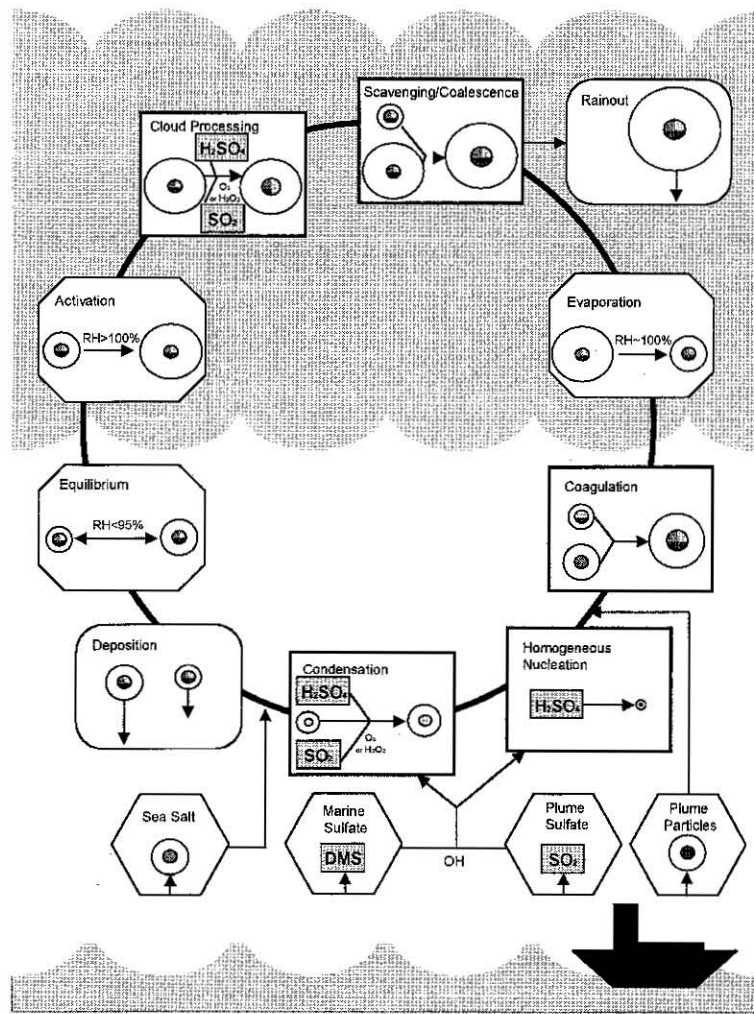
Figure 1. Diagram of chemical and microphysical processes included in the Princeton model of a ship track. Mechanisms in rectangles indicate processes causing aerosol growth. Mechanisms in rectangles with flattened corners represent processes that change the ambient size of particles by addition or removal of water. Mechanisms in rectangles with rounded corners show processes for particle removal. Fluxes from natural and anthropogenic sources are shown in hexagons.

some particles of dissimilar compositions (for example, "pure" salt particles with salt particles onto which non-sea-salt sulfate has condensed) in the same category. However, we believe it is preferable to the approach of *Jacobson et al.* [1994] in which all coagulated particles are placed into a single "mixed" population retaining no distinction between particles of different compositions, since over time this category will represent an increasing fraction of the particle number, thus failing to preserve the external mixture properties of the original scheme.

Aerosol microphysics, gas-phase and heterogeneous sulfur chemistry, and boundary layer concentration and temperature gradients are described explicitly (see Figure 1). The model employs a fixed sectional representation of the size domain with a dual moment (number and mass) algorithm to calculate growth of particles from one section to the next for nonevaporating species (namely, all components other than water). Water is treated in a moving section representation, similar to

the approach of *Jacobson et al.* [1994], to allow the accurate calculation of evaporation and condensation of water in conditions of varying humidity.

The model uses a dual moment method based on *Tzivion et al.* [1987] to allow accurate accounting of both aerosol number and mass. This algorithm incorporates independent calculations of the change in particle number and mass for all processes other than growth. For particle number,

$$\frac{dN_{\mathrm{P}ik}}{dt} = J_{ik}^{\mathrm{nucl}} + J_{ik}^{\mathrm{flux}} - K_{ik}^{\mathrm{depn}} N_{\mathrm{P}ik} + J_{ik}^{\mathrm{grow}}$$

$$+ \frac{1}{2} \sum_{i_1 \leq i} \sum_{i_2 \leq i} \sum_{k_1 \leq k} K_{i_1 i_2}^{\mathrm{coag}} N_{\mathrm{P}i_1 k_1} N_{\mathrm{P}i_2 k}$$

$$- \sum_{i_1 \leq i_{\max}} \sum_{k_1 \leq k_{\max}} K_{i_1 i}^{\mathrm{coag}} N_{\mathrm{P}i_1 k_1} N_{\mathrm{P}ik}, \quad (1)$$

where $N_{\mathrm{P}ik}$ is the number of particles in size section i of particle population k. Here J_{ik}^{nucl}, J_{ik}^{flux}, and J_{ik}^{grow} are

the rates of particle production by nucleation, transport from external sources, and growth to other size bins, respectively. The rate constants for deposition and coagulation are K_{ik}^{depn} for particles with the ambient size of section i in population k and $K_{i_1 i_2}^{\text{coag}}$ between particles with the ambient sizes of sections i_1 and i_2. The change in particle mass, including condensational growth, is then described by

$$
\begin{aligned}
\frac{\partial M_{\text{P}ijk}(t)}{\partial t} = {} & \frac{M_{\text{P}ijk}}{\sum_j M_{\text{P}ijk}} m_{ik} J_{ik}^{\text{nucl}} \\
& + \frac{M_{\text{P}ijk}}{\sum_j M_{\text{P}ijk}} m_{ik} J_{ik}^{\text{flux}} \\
& - \frac{M_{\text{P}ijk}}{\sum_j M_{\text{P}ijk}} m_{ik} K_{ik}^{\text{depn}} N_{\text{P}i} \\
& + \frac{M_{\text{P}ijk}}{\sum_j M_{\text{P}ijk}} m_{ik} J_{ik}^{\text{grow}} \\
& + \frac{1}{2} \frac{M_{\text{P}ijk}}{\sum_j M_{\text{P}ijk}} m_{ik} \\
& \quad \times \sum_{i_1 \le i} \sum_{i_2 \le i} \sum_{k_1 \le k} K_{i_1 i_2}^{\text{coag}} N_{i_1 k_1} N_{\text{P}i_2 k} \\
& - \frac{M_{\text{P}ijk}}{\sum_j M_{\text{P}ijk}} m_{ik} \\
& \quad \times \sum_{i_1 \le i_{\max}} \sum_{k_1 \le k_{\max}} K_{i_1 i}^{\text{coag}} N_{\text{P}i_1 k_1} N_{\text{P}ik} \\
& + 2\pi \mathcal{D}_j D_{\text{P}ik}^{\text{amb}} F(\text{Kn}_{ik}) A(\text{Kn}_{ik}) \\
& \quad \times (P_j^{\infty} - P_{ijk}^{\text{surf}}), \qquad (2)
\end{aligned}
$$

where $M_{\text{P}ijk}$ is the mass of species j in section i of particle population k, and m_{ik} is the mass of a single particle of population k, in section i. In this expression, $\mathcal{D}_j$, P_j^{∞}, and P_{ijk}^{surf} are the diffusivity, bulk partial pressure, and surface partial pressure of vapor-species j, $D_{\text{P}ik}^{\text{amb}}$ and Kn_{ik} are the ambient diameter and associated Knudsen number of particles in section i of population k, and the correction factors $F(\text{Kn}_{ik})$ and $A(\text{Kn}_{ik})$ account for free molecular effects and mass transfer limitations, respectively.

3.1. Nucleation

The binary, homogeneous nucleation rate for sulfuric acid and water is calculated on the basis of *Kulmala and Laaksonen* [1990]. We consider vapor-phase oxidation of DMS to SO_2 with a yield of 80% and of SO_2 to H_2SO_4 [*Pandis et al.*, 1994]. Aqueous oxidation of SO_2 is assumed to be limited by the rate of transfer of SO_2 from the vapor as long as an oxidant is available. In the absence of size-segregated information about the distribution of the primary potential aqueous oxidants, H_2O_2 and O_3, we have used a midrange value of 10 μM H_2O_2 from the measured cloud concentrations of *Richards et al.* [1983] and have taken O_3 available for oxidation to be in excess since the presence of sufficient

ammonia keeps the pH from becoming too acidic. As a result, aqueous oxidation of SO_2 was limited largely by the particulate surface area controlling the impingement rate of molecules. Also, the sulfuric acid activity of the particle was assumed to be negligible, making surface area the limiting factor for the H_2SO_4 condensation rate.

3.2. Fluxes

To identify the potential of particles to act as CCN, the chemical and microphysical properties of the vapor and aerosol phases must be described. Here we have used measurements from the MAST experiment to provide initial conditions for particle size distributions and for SO_2 concentrations. Ambient particle and vapor concentrations for the case studies here are described in section 4. DMS and H_2SO_4 were not measured and have been initialized by marine boundary layer mixing ratios of 5 parts-per-trillion (ppt) and 0 ppt, respectively [*Pandis et al.*, 1994], in accordance with measurements in temperate marine conditions [*Bates et al.*, 1990; *Weber et al.*, 1995; *DeBruyn et al.*, 1998]. A conservative value for marine DMS flux of 2 μmol m^{-2} d^{-1} is used on the basis of low wind speeds in clouded conditions in the midlatitude Pacific Ocean [*Bates et al.*, 1987]. The average ion ratio of NH_4^+ to SO_4^{2-} is based on a midlatitude eastern Pacific Ocean average value of 1.5 [*Quinn et al.*, 1990].

Filter measurements of submicron aerosol ionic compositions were collected [*Hobbs et al.*, 2000], but size-resolved information for each externally mixed particle population was not measured. "Sea salt" particles are considered to be primarily sodium chloride, and DMS-derived "marine sulfate" particles are dominated by ammonium sulfate and bisulfate. Since the stack dilution conditions are not known, "plume" emissions are estimated to be mixtures of 50% organic carbon and 50% black carbon (consistent with the range of compositions measured by *Hildemann et al.*[1991]), where all sulfur dioxide produced in stack combustion and emitted with the particles is assumed to be in the vapor phase at stack exit, although it condenses rapidly during the initial period of the simulation. While this assumption neglects the sulfur vapors that condense prior to exiting the stack, it is useful in providing an artificial distinction between primary and secondary particle mass. "Continental" emissions are taken to be a mixture of several combustion sources (including industrial boilers and automobiles), onto which coemitted sulfur species have already condensed, resulting in internal mixtures of 50% ammonium sulfate and bisulfate, 25% organic carbon, and 25% black carbon [*Hildemann et al.*, 1991].

3.3. Deposition

Particle deposition is calculated from the gravitational settling velocity based on the ambient size and density of particles of type k in size bin i [*Seinfeld and*

Pandis, 1998]. Since water is not included in the mass used to represent the fixed-section grid, the ambient diameter of particles does not correspond to the grid (dry) diameters. The following identity illustrates this important distinction:

$$D_{\mathrm{P}ik}^{\mathrm{amb}}(t) = \left(\frac{\sum_j M_{\mathrm{P}ijk}(t)}{\frac{\pi}{6}\rho_{\mathrm{P}ik}(t)N_{\mathrm{P}ik}(t)} \right)^{\frac{1}{3}}, \qquad (3)$$

where the ambient diameter of particles and droplets is $D_{\mathrm{P}ik}^{\mathrm{amb}}$ for section i of population k. Consequently, at each time step for each section of each particle type, an ambient diameter is calculated on the basis of the total mass of all species present and their volume-weighted densities. The ambient diameter is then used in order to calculate the slip correction factor needed for deposition, as well as the surface area available for condensation and the collision cross section needed for coagulation.

3.4. Growth

Growth of particles, described by the term J_{ik}^{grow}, is evaluated as a net contribution to each section by evaluating the remaining terms of equations (1) and (2) subject to conservation of the zeroth and third moments between adjacent sections, namely for section i and section $i+1$,

$$N_{\mathrm{P}ik}(t) = \frac{\sum_{j,j\neq H_2O} M_{\mathrm{P}ijk}(t)}{\frac{\pi}{6}\rho_{\mathrm{P}ik}(t)\left(D_{\mathrm{P}i}^{\mathrm{dry}}\right)^3}, \qquad (4)$$

$$N_{\mathrm{P}(i+1)k}(t) = \frac{\sum_{j,j\neq H_2O} M_{\mathrm{P}(i+1)jk}(t)}{\frac{\pi}{6}\rho_{\mathrm{P}(i+1)k}(t)\left(D_{\mathrm{P}i+1}^{\mathrm{dry}}\right)^3}, \qquad (5)$$

where $D_{\mathrm{P}i}^{\mathrm{dry}}$ is the mass mean diameter of dry components of section i and is fixed during the simulation such that

$$\frac{D_{\mathrm{P}(i+1)}^{\mathrm{dry}}}{D_{\mathrm{P}i}^{\mathrm{dry}}} = \mathrm{constant}. \qquad (6)$$

In some cases the accuracy of this approach is limited by numerical diffusion [*Jacobson*, 1997], but for the number concentrations and growth rates considered over the time scales of 20 min to 75 min (corresponding to updraft velocities of 0.5 m s^{-1} to 0.2 m s^{-1}) used here, these errors are negligible.

Tracking changes in particle size requires careful attention in numerical models of aerosol populations. Since the particle number distribution determines the number of nuclei available for cloud droplet formation, conservation of particle number in the calculation of growth and coagulation is critical to modeling cloud processes such as those involved in ship tracks, especially since ship tracks are characterized by significant changes in number concentrations of interstitial aerosol and cloud droplets. When discrete size sections are used, artificial diffusion of particles among adjacent size bins can occur [*Wexler and Seinfeld*, 1990; *Dhaniyala and Wexler*, 1996]. Even accurate advection algorithms, such as accurate space derivatives [*Wexler and Seinfeld*, 1990] and the Bott method [*Bott*, 1989] can fail to conserve particle number by apportioning additional mass to a particle number in a fixed size bin. For these studies we have determined that numerical diffusion is negligible for the duration of the events studied, corresponding to timescales of up to 2 hours, by confirming that the number and shape of the size distribution are conserved by the model in the absence of both condensation and coagulation. We have employed 40 size bins in the dry diameter range of 0.005 μm to 50.0 μm. The time step was varied from 1 s to 10 s where the shorter time steps were needed to follow water condensation in updrafts, and longer time steps were used when water was partitioned at equilibrium below cloud.

3.5. Coagulation

Coagulation is treated by an algorithm that considers particles to have a comparatively involatile core substance, so coagulated particles are assigned to one of the original particle types based on the least volatile core component [*Russell and Seinfeld*, 1998]. This approach assigns "mixed" particles to different bins and allows the original composition of particle types to change, while retaining characteristics that could be compared to volatility-based measurements.

3.6. Condensation

The model includes a dynamic scheme for activating particles to cloud droplets [*Russell and Seinfeld*, 1998]. In subsaturated conditions below cloud base aerosol particles can be considered to be in local equilibrium with water vapor; for the conditions of the MAST experiment, the characteristic time to reach water vapor equilibrium is always less than 1 s. The surface area used in calculating condensation rate accounts for the water associated with each particle dry mass by using the ambient particle diameter defined by equation (3). Our predictions assume that these thermodynamic parameters are the ones on which aerosol particles have a negligible feedback effect due to small associated changes in the heat of condensation evolved and in the density and viscosity of the nondrizzling particle-laden air parcel.

4. Case Studies

A clean marine case and a continentally influenced case were chosen to represent the different ambient conditions and ship emissions sampled during MAST: (1) *Star Livorno*, University of Washington (UW) C131-A flight 1648, June 29 (JDT 180) (clean marine case);

Table 1. Measured and Estimated Track and Background Conditions for the Clean Marine Case (JDT 180) and the Continentally Influenced Case (JDT 178)

	Clean Marine Case		Continentally Influenced Case	
	Background	Track	Background	Track
Case Description				
Ship	*Star Livorno*		*Tai He*	
Date	June 29, 1994		June 27, 1994	
Julian Date (JDT)	180.51 to 180.60		178.49 to 178.55	
Latitude	36.1°N to 37.3°N		35.5°N to 35.8°N	
Longitude	-125.3°W to -126.3°W		-123.4°W to -123.9°W	
Thermodynamic Quantities				
Boundary layer height (m)	450	450	405	405
Cloud base (m)	230	230	173	173
Cloud base temperature (K)	273.7	273.7	285.3	285.3
Lapse rate (K km^{-1})	6.5	6.5	6.1	6.1
Total water content (g m^{-3})	10.3	10.3	11.4	11.4
Wind speed (m s^{-1})	12	12	12	12
Microphysical Characteristics				
Updraft velocity (m s^{-1})	0.3±0.2	0.3±0.2	0.3±0.2	0.3±0.2
Cloud droplet number (cm^{-3})	49±10	110±32	132±41	162±37
Liquid water content (g m^{-3})	0.28±0.05	0.31±0.11	0.35±0.05	0.35±0.05
Effective radius (μm)	7.87	5.10	5.98	5.67
Chemical Species				
SO$_2$ (ppb)	0.34	3.7	1.0	6.5
NO (ppb)	0	0.3	0	0
NO$_2$ (ppb)	0.44	0.05	0.29	0.18
HCHO (ppb)	0.1	2	1	2
O$_3$ (ppb)	26	21	25	27
CO$_2$ (ppb)	360	360	360	360
OH (ppb)	1.43x10^{-6}	3.77x10^{-7}	6.42x10^{-7}	4.41x10^{-7}
H$_2$O$_2$ (μM)	88	88	88	88
H$_2$SO$_4$ (ppt)	0	0	0	0
DMS (ppt)	5	5	5	5
DMS flux (μmol m^{-2} d^{-1})	2	2	2	2
Aerosol Populations				
Total aerosol (cm^{-3})	104	18528	1113	2894
Primary mode peak (μm)	0.08	0.05	0.4	0.4
Secondary mode peak (μm)	NA	0.2	0.07	0.06
Marine sulfate aerosol (cm^{-3})	94	94	81	81
(NH$_4$)$_2$SO$_4$ mass (dry)	53%	53%	53%	53%
(NH$_4$)HSO$_4$ mass (dry)	47%	47%	47%	47%
Sea Salt aerosol (cm^{-3})	10	10	10	10
NaCl mass (dry)	100%	100%	100%	100%
Plume aerosol (cm^{-3})	0	18424	0	1781
OC mass (dry)	NA	50%	NA	50%
EC mass (dry)	NA	50%	NA	50%
Continental aerosol (cm^{-3})	0	0	1022	1022
(NH$_4$)$_2$SO$_4$ mass (dry)	NA	NA	25%	25%
(NH$_4$)HSO$_4$ mass (dry)	NA	NA	25%	25%
OC mass (dry)	NA	NA	25%	25%
EC mass (dry)	NA	NA	25%	25%

"NA" indicates that this composition is not applicable since there were no particles present of this type for this case.

and (2) *Tai He*, UW C131-A flight 1646, June 27 (JDT 178) (continentally influenced case). The *Tai He* case illustrates ship tracks in continentally influenced marine air, in which the in-track aerosol signal was weak and the ship track was only faintly visible in satellite imagery [*Noone et al.*, 2000b; *Hobbs et al.*, 2000]. The *Star Livorno* was sampled in clean marine conditions with low background aerosol concentrations [*Hobbs et al.*, 2000]. The *Tai He* and *Star Livorno* were studied primarily with instrumentation aboard the UW C131-A

[Russell et al., 1995, 1996; *Hobbs et al.*, 2000], although the MRF C130 flew near similar tracks in adjacent regions on the same days [*Hobbs et al.*, 2000].

Case studies incorporating data of simultaneous measurements of microphysical, chemical, and meteorological parameters from the MAST experiment appear elsewhere [*Durkee et al.*, 2000b; *Noone et al.*, 2000a, b; *Hobbs et al.*, 2000]. Supporting information about the MAST operations and the ships sampled during the study are described by *Gasparovic* [1995].

The case studies of clean marine (JDT 180) and continentally influenced (JDT 178) conditions illustrate the range of conditions measured during the MAST experiment. For each case, the measured and estimated conditions used to initialize the prediction of the evolution of particle size are shown in Table 1, with the initial particle number and mass distributions described below. In both cases, comparing the evolution of particles in background aerosol and in track conditions allows comparison of the influence of particle conditions under essentially identical meteorological forcing. Here the background conditions provide an experimental control for comparison to the track conditions.

There are two main microphysical differences between the two cases studied. The background cases differ in that particle size distributions measured on JDT 178 show a clear influence of continentally derived anthropogenic particles in background air. In addition, the apparent source strength of the particles emitted by the *Tai He* is significantly less than that for the *Star Livorno*, as can be seen from the significantly larger number of particles measured on JDT 180 than on JDT 178. The resulting track is characterized by a relative change in particle number and mass that is smaller in the continentally influenced case than in the case with a clean marine background. There are also minor differences in the boundary layer structure in the two cases, including a slightly higher but almost identical in thickness cloud on JDT 180.

Particle populations in the initial size distribution are assigned by estimating the basic sea salt contribution and assigning the remaining clean marine submicron particles to the marine sulfate population. Plume particles are determined by the difference between the total plume particle number size distribution for each case and the total background size distribution for that case (namely, sea salt particles plus marine sulfate particles). Continentally derived particles are assigned as those present in the (background) continentally influenced case which exceed the number distribution of particles present in the (background) clean marine case.

In this section, we describe predictions of cloud formation for the cases studied, with cloud characteristics for each case summarized in Table 2. All simulations were run for one complete cycle through the boundary layer, which was equivalent to about 50 min for the

Table 2. Predicted Cloud and Aerosol Characteristics for Track and Background Conditions for the Clean Marine Case (JDT 180) and the Continentally Influenced Case (JDT 178)

| | Clean Marine Case | | | | Continentally Influenced Case | | | |
| | Background | | Track | | Background | | Track | |
	Updraft Only	Cloud Average	Updraft Only	Cloud Average	Updraft Only	Cloud Average	Updraft Only	Cloud Average
Cloud Properties								
Liquid water content (g m^{-3})	0.34	0.19	0.36	0.20	0.39	0.22	0.39	0.22
Effective radius (μm)	10.8	10.8	3.4	3.4	5.7	5.7	4.1	4.1
Droplet number (cm^{-3})	96	48	3880	2130	533	293	1790	985
Maximum supersaturation	0.68%	NA	0.18%	NA	0.26%	NA	0.15%	NA
Droplet Populations (>1 μm)								
Marine sulfate droplets (cm^{-3})	86	47	48	26	55	30	52	29
Sea salt droplets (cm^{-3})	10	6	7	4	7	4	6	3
Plume droplets (cm^{-3})	0	0	3820	2101	0	0	1270	699
Continental droplets (cm^{-3})	0	0	0	0	471	259	471	259
Aerosol Populations (total)								
Marine sulfate aerosol (cm^{-3})	94	94	93	93	81	81	81	81
Sea Salt aerosol (cm^{-3})	10	10	10	10	10	10	10	10
Plume aerosol (cm^{-3})	0	0	18300	18300	0	0	1750	1750
Continental aerosol (cm^{-3})	0	0	0	0	1020	1020	1010	1010
Aerosol Species (<1 μm)								
$(NH_4)_2SO_4$ mass (μg m^{-3})	0.88	0.88	10.4	10.4	3.8	3.8	17.9	17.9
$(NH_4)HSO_4$ mass (μg m^{-3})	0.78	0.78	9.3	9.3	3.3	3.3	15.9	15.9
OC mass (μg m^{-3})	0	0	1.51	1.51	0.90	0.90	1.36	1.36
EC mass (μg m^{-3})	0	0	1.52	1.52	0.90	0.90	1.36	1.36

Values are given both for the updraft predictions (in the column labeled "Updraft Only") and the estimated average assuming a cloud updraft area fraction of 55% (in the column labeled "Cloud Average").
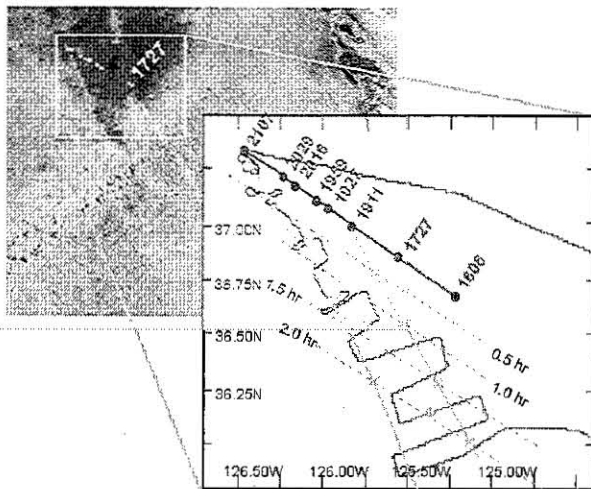
Figure 2. AVHRR image from the 3.7 μm channel at 1026 PDT on June 29, 1994, for the clean marine stratocumulus cloud case (JDT 180). The ship position is shown with white dots on the satellite image and with gray dots and labeled position times on the magnified inset. The inset also shows the flight track of the University of Washington C131-A aircraft as a black line with gray dots where the track was sampled. Times labeling dashed gray lines indicate the approximate age of the track measured from the time of emission to the sampling point. Solid gray lines show the observed track location at the indicated satellite overpass times.

base case updraft velocity of 0.3 m s^{-1} [*Nicholls and Leighton*, 1986].

4.1. Clean Marine Case: *Star Livorno*, June 29 (JDT 180)

Figure 2 illustrates the cloud reflectance for the ship track measured on June 29, 1994. The particle number concentration measured was 104 cm^{-3}, indicative of clean marine air [*Hoppel et al.*, 1990]. The aerosol in the plume of the *Star Livorno* was characterized by a peak at 0.05 μm (dry) diameter as measured directly after emission from the stack below cloud. The associated track measured in cloud was characterized by a corresponding peak of interstitial particles at 0.05 μm (dry) diameter. Over the length of track sampled (from <1 hour to 2.5 hours after emission from the ship), particles from the mode between 0.030 and 0.100 μm diameter were depleted.

The vertical temperature profile for the cloud sampled on this day is shown in Figure 3. The below-cloud temperature was extrapolated from the lowest flight altitude (∼ 50 m) to the surface as a constant temperature since the surface conditions were not measured directly. The temperature profile corresponds to an average lapse rate in the cloud layer of 6.5 K km^{-1}. Total water content of the boundary layer air was measured to be approximately constant below cloud at 10.25 g m^{-3}. Measured particle and cloud droplet distributions

collected near the top of the cloud layer are shown in Figure 4. As a result of the significant variability along the length and width of the ship track, with values of liquid water content varying between 0.2 and 0.5 g m^{-3}, there is no statistically significant distinction between background and track values of liquid water. There is also no clear trend in liquid water with track age.
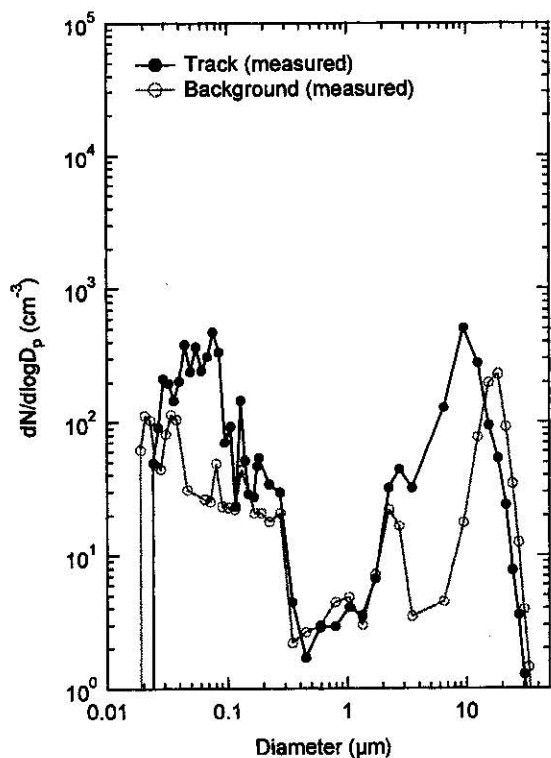
In the clean marine case study, the background particle size distribution is composed entirely of sea salt and marine sulfate particles with a mean particle number concentration of 104 cm^{-3}. Contrasting this distribution to the track initial size distribution in this case shows the track distribution dominated by over 18,400 cm^{-3} plume particles. This large particle number was measured close to (within 100 m) the stack of the *Star Livorno*. The resulting factor of over 100 increase in particle concentration also overwhelms the cloud droplet distribution during the initial cloud cycle, even though more dilution will occur before the parcel reaches cloud base than we have assumed in the initial case study.

4.1.1.   Predicted background aerosol. The particle size distribution below cloud initialized from
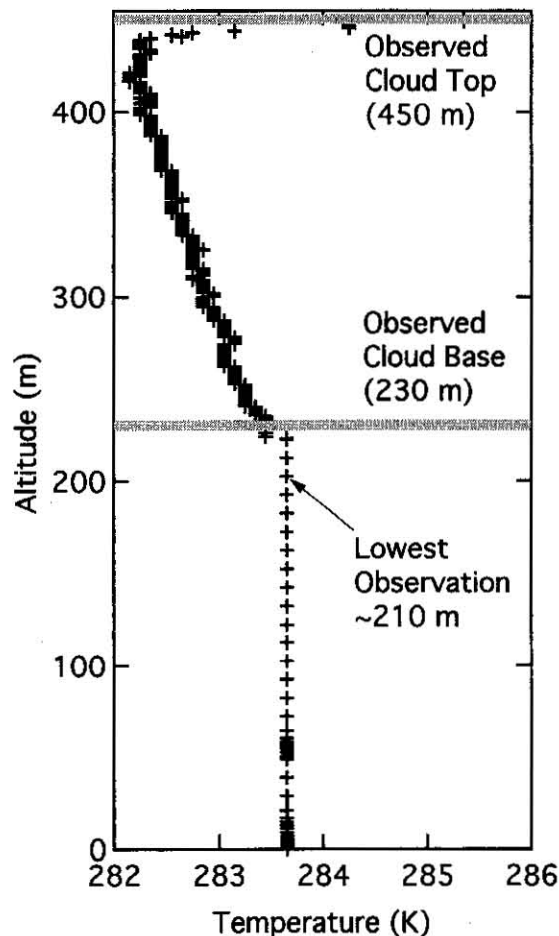
Figure 3. Measured temperature profile for the clean marine cloud case (JDT 180). Pluses indicate data measured during a profile through the boundary layer by the University of Washington C131-A aircraft.
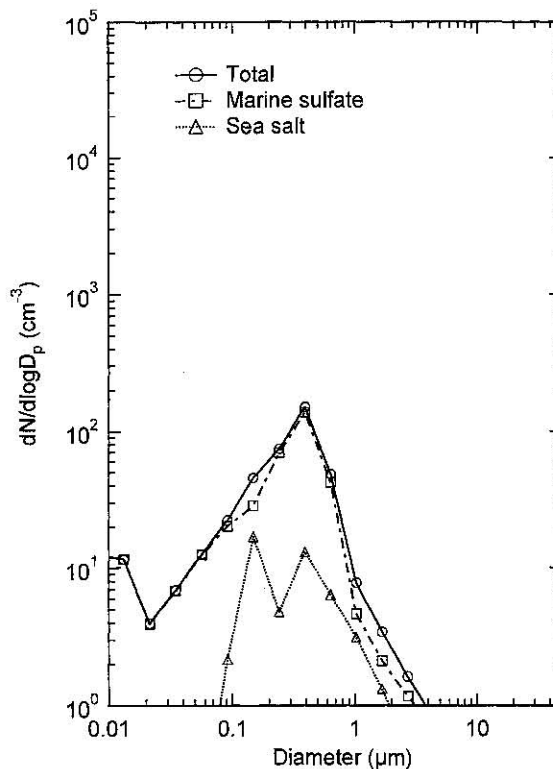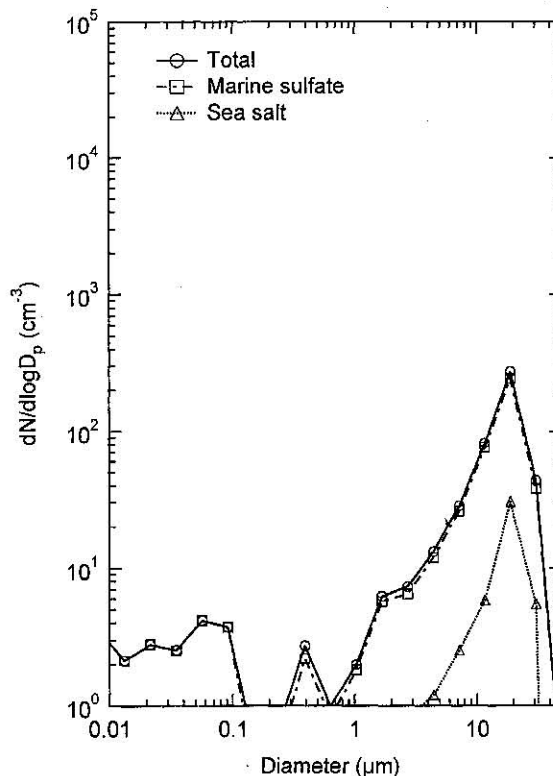
Figure 4. Measured in-cloud particle and droplet size distribution for track and background clouds in the clean marine case (JDT 180). Solid circles represent track cloud measurements and open circles represent background cloud measurements.

Figure 5. Predicted below-cloud particle size distribution for background air in the clean marine case (JDT 180). Circles show the total aerosol number distribution, squares show marine sulfate particles, and triangles show sea-salt particles.

the measured aerosol concentration is shown in Figure 5. As particles are activated in the updraft region at a prescribed velocity of 0.3 m s^{-1}, the maximum supersaturation attained is 0.68%, which is shown in Figure 7. The resulting in-cloud distribution of particles and droplets is shown in Figure 6. Of the 96 cm^{-3} predicted to be activated to cloud droplets, 86 cm^{-3} are marine sulfate particles and 10 cm^{-3} are sea-salt particles (Table 2).

The predicted droplet distribution of the cloud has a vertically averaged liquid water content of 0.34 g m^{-3} and effective radius of 10.8 μm. The predicted liquid water in the updraft is greater than the average measured liquid water content for this cloud of 0.28 g m^{-3}, but since the measured value reflects an average in the cloud rather than in just the updraft, we have also included in Table 2 an estimate of the cloud average, assuming that updrafts represent 55% of the cloud area and downdrafts account for the remaining 45% [de Laat and Duynkerke, 1998]. The predicted average for the cloud with 55% updraft fraction is only 0.19 g m^{-3}, which is below the measured value. Both are within the range of the values measured in cloud. It is interesting to note that the predicted number of droplets of 48 cm^{-3} for the cloud average is almost identical to the reported number of measured droplets (49 cm^{-3}).

Figure 6. Predicted in-cloud particle and droplet size distribution for background cloud in the clean marine case (JDT 180). Symbol definitions are the same as in Figure 5.
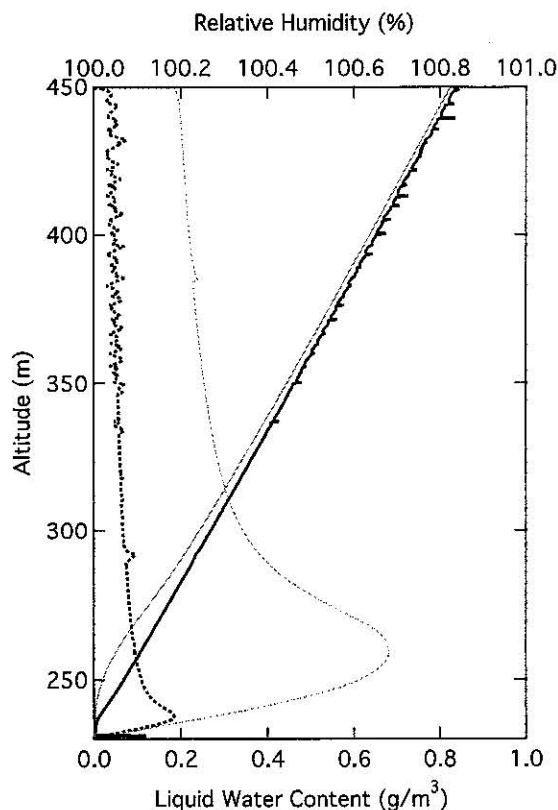
Figure 7. Predicted profile of liquid water content and relative humidity (supersaturated) for the clean marine case (JDT 180) for background and track clouds. Thin solid line shows liquid water content in background cloud, and thick solid line shows liquid water content in track. Thin dashed line shows relative humidity in background cloud, thick dashed line shows relative humidity in track.

4.1.2. Predicted track aerosol. In track the plume aerosol population provides so many particles that can act as CCN that almost all of the resulting cloud droplets are predicted to have plume particles as nuclei. Particles available to act as CCN are shown in the below-cloud size distribution in Figure 8. The high number of CCN available results in more droplets activating sooner in cloud, consequently depleting the supply of water available to condense, so a maximum supersaturation of only 0.18% is reached (Figure 7) for the track case ∼ 20 m below the maximum supersaturation altitude in the background cloud.

Average droplet distribution in cloud for the track is shown in Figure 9. The effective cloud droplet radius predicted in this case, 3.4 μm, is significantly smaller than the observed ambient cloud. This size range corresponds to the smallest channel of cloud probes, in which significant uncertainties exist. Liquid water is increased to an average value of 0.36 g m^{-3} in track, an increase of 0.02 g m^{-3} from the background, as can be seen in Figure 7.

Measured submicron aerosol size distributions show a depletion of particles at 0.1 μm (dry) diameter and

simultaneous appearance of particles at larger sizes 0.2-0.3 μm (dry) diameter as the track ages. This change is consistent with the predicted activation of particles at this size range as well as with the growth of the emitted plume particles by below-cloud H$_2$SO$_4$ condensation.

4.2. Continentally Influenced Case: *Tai He*, June 27 (JDT 178)

The signature of the ship track from the *Tai He* in continentally influenced air measured on June 27 (JDT 178) is faintly visible in the AVHRR 3.7 μm channel image shown in Figure 10. The stratus cloud on this flight was characterized by high levels of background particles as indicated by the condensation nuclei and cloud droplet number measurements reported [*Gasparovic*, 1995]. The background aerosol is characterized by two modes, one at 0.4 μm (dry diameter) and a smaller mode at 0.07 μm, with concentration of 1110 cm^{-3}.

The plume of the *Tai He* exhibited a peak at 0.06 μm. In cloud the track of the *Tai He* was characterized by increased interstitial aerosol and a minor mode at 0.01 μm (dry diameter). The cloud measured for this case is very similar to the JDT 180 case in thickness but was approximately 50 m lower, extending from 175 m above sea level to 405 m. The measured temperature
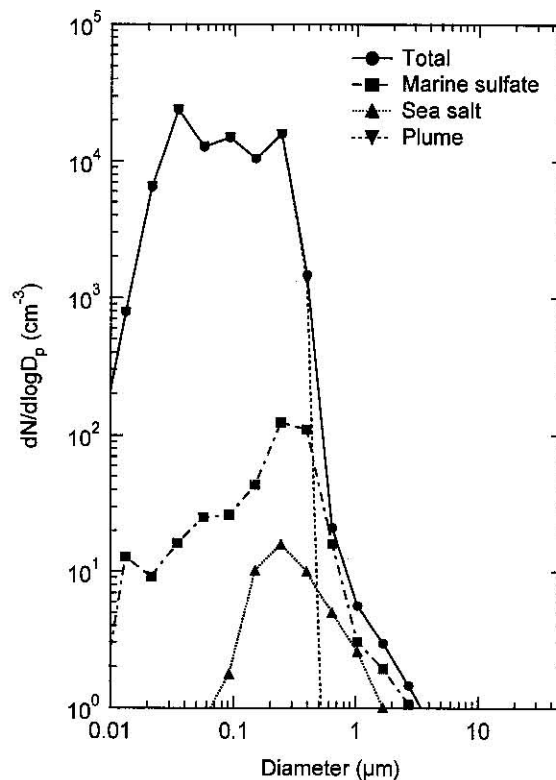

Figure 8. Predicted below-cloud particle size distribution for track air in the clean marine case (JDT 180). Circles show the total aerosol number distribution, squares show marine sulfate particles, triangles show sea salt particles, and inverted triangles show plume particles.
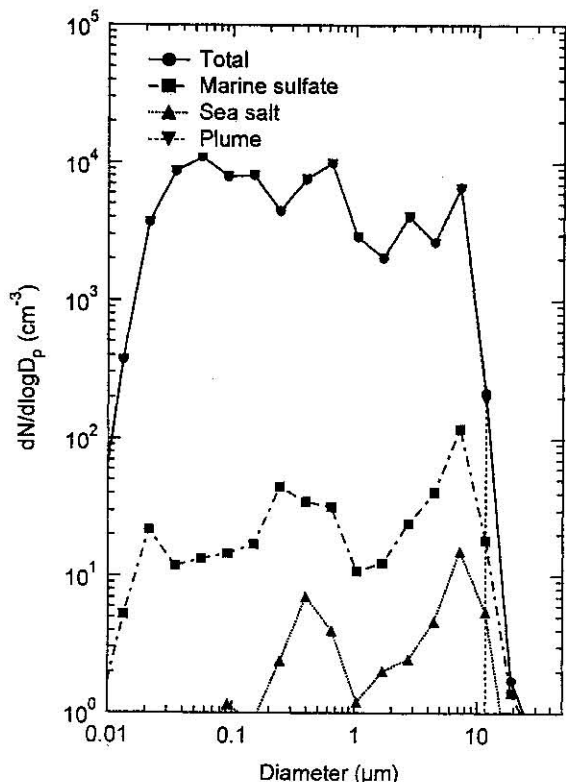
Figure 9. Predicted in-cloud particle and droplet size distribution for track air in the clean marine case (JDT 180). Symbol definitions are the same as in Figure 8.

profile shows an average lapse rate of 6.1 K km^{-1} in the cloud layer (Figure 11). Distributions of particles and droplets in the cloud are shown in Figure 12. Below cloud level, the total water content of the boundary layer air was measured to be 11.4 g m^{-3}. The liquid water measured in this case was less variable in both the track and the background cloud, with an average value of 0.35 g m^{-3}.
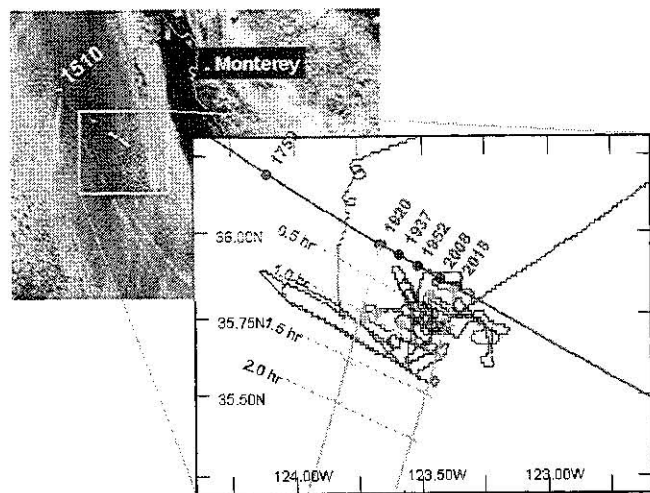
Figure 10. Same as Figure 2 at 0810 PDT on June 27, 1994, for the continentally influenced case (JDT 178) with the *Tai He*.
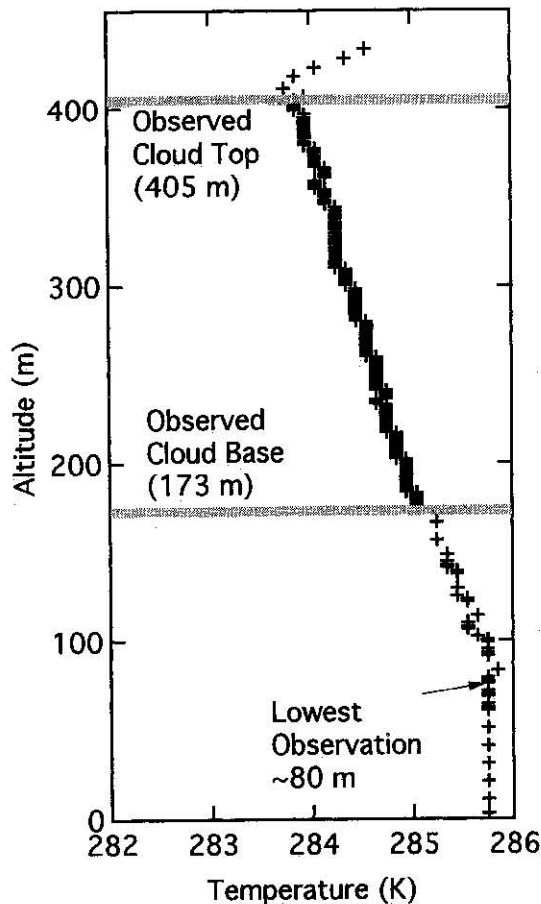

Figure 11. As for Figure 3 but for the continentally influenced cloud case (JDT 178).

The presence of continentally influenced background air on JDT 178 resulted in increased background concentrations of SO$_2$ and particles. Because many of the particles in this case are aged combustion particles from continental sources (and hence constitute the continental aerosol population), they are represented in the model by a composition that is 50% carbonaceous and 50% condensed sulfur species (ammonium sulfate and ammonium bisulfate), as summarized in Table 1. These continentally derived particles are larger than the sea salt and more numerous than the marine sulfate particle populations.

4.2.1. Predicted background aerosol. The initial below-cloud particle size distribution for background conditions on JDT 178 is shown in Figure 13. Particle number is dominated by continentally derived aerosol, although sulfate aerosol constitutes a fraction of particles large enough to act as CCN. When the air parcel reaches cloud base and becomes supersaturated, the predominant number of particles activated to droplets are continentally derived as shown in Figure 14.

Throughout the vertical extent of this cloud, liquid water increases monotonically as shown in Figure 15, and supersaturation reaches a maximum of 0.26%. The average effective radius over the cloud depth is 5.7 μm with an associated liquid water of 0.39 g m^{-3} in up-
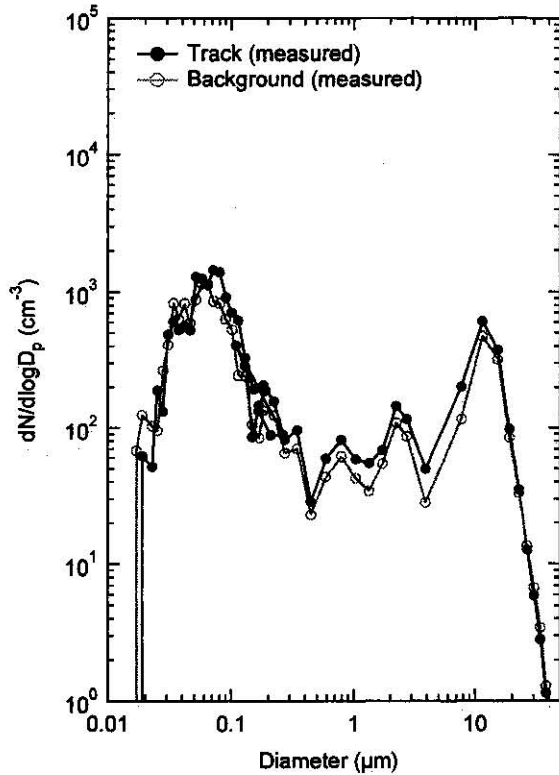
Figure 12. Measured in-cloud particle and droplet size distribution for track and background clouds in the continentally influenced case (JDT 178). Symbol definitions are the same as in Figure 4.
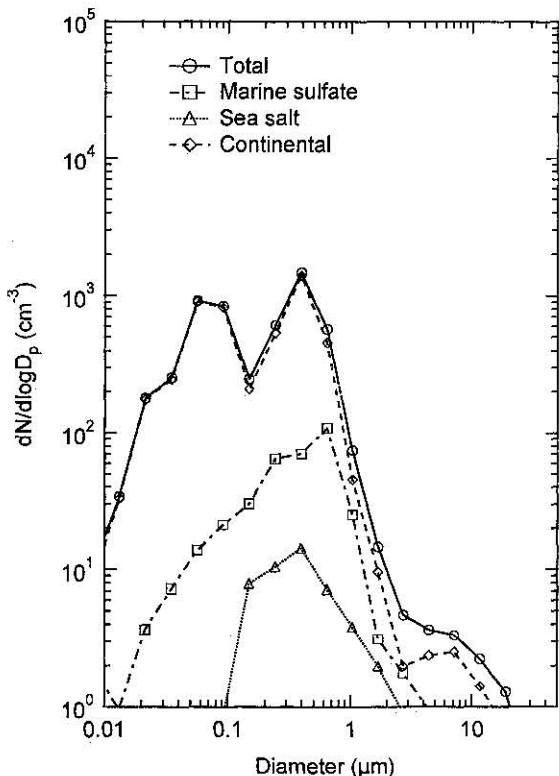
Figure 13. Predicted below-cloud particle size distribution for background air in the continentally influenced case (JDT 178). Circles show the total aerosol number distribution, squares show marine sulfate particles, triangles show sea-salt particles, and diamonds show continental particles.
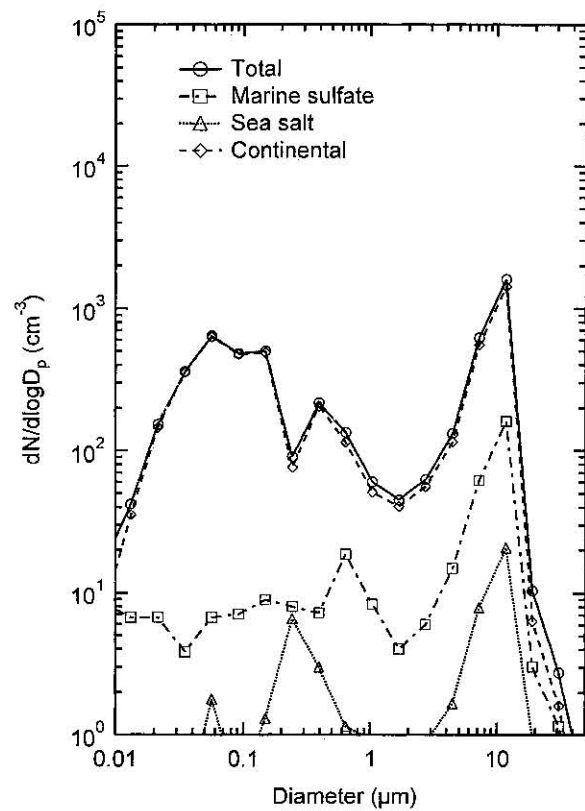
Figure 14. Predicted in-cloud particle and droplet size distribution for background air in the continentally influenced case (JDT 178). Symbol definitions are the same as in Figure 13.

drafts or 0.22 g m^{-3} averaged in the cloud. The measured liquid water of 0.35 g m^{-3} falls between these two predicted values, but both predictions are within the range of liquid water content reported in cloud.

4.2.2. Predicted track aerosol. In the track in cloud, plume particles represent over half of the particle number distribution. Below-cloud particle number distribution and the contribution from different particle populations are shown in Figure 16. The activated droplet distribution is shown in Figure 17 including only a significant fraction of activated particles from plume particles, with almost all (1010 cm^{-3} in track compared to 1020 cm^{-3} in the background) of the continental particles that activated in the background case also forming droplets here.

Predicted cloud water characteristics for the track on JDT 178 are only slightly different from the background case, with an average liquid water remaining at 0.39 g m^{-3} and a maximum supersaturation of 0.26% in the background decreasing slightly to 0.15% in track, as illustrated in Figure 15. Despite the small changes from the background to the track in liquid water and maximum supersaturation, the cloud effective radius decreases from 5.7 μm to 4.1 μm and cloud droplet number more than triples from 533 cm^{-3} to 1790 cm^{-3}. While these changes do alter the albedo [*Erlick et al.*, 1999], they are small compared to the changes predicted in the
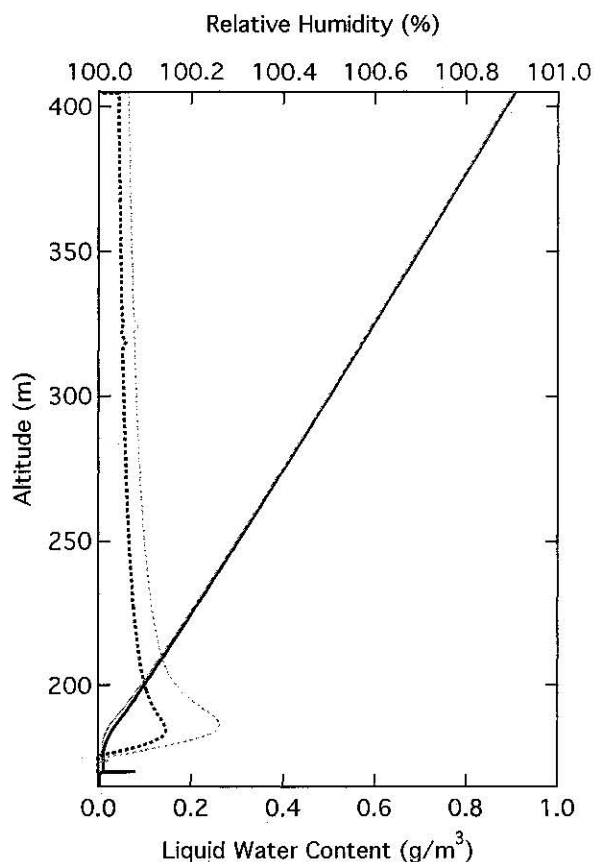
Figure 15. As for Figure 7 but for the continentally influenced case (JDT 178).

itation, we have modeled one case with the DESCAM (detailed scavenging and microphysics) cloud dynamics and microphysics model from the Clermont-Ferrand group [*Flossmann et al.*, 1985].

5.1. Gas-to-Particle Conversion

A microphysical mechanism that may be of importance in ship tracks is gas-to-particle conversion, encompassing processes from nucleation to homogeneous and heterogeneous oxidation [*Ferek et al.*, 1998]. *Ferek et al.* [1998] studied measurements of ship tracks off the coast of Washington and found that gas-to-particle conversion, possibly in combination with increases in cloud peak supersaturation, may account for ship track persistence. These processes contribute to aerosol size distribution dynamics and influence the nature of their cloud interactions. The size and composition of CCN available will influence the maximum cloud supersaturation, liquid water content, and droplet distribution, and hence the radiative features that characterize ship tracks. Here we consider separately the role of these processes in forming and maintaining tracks.

In the formation of a ship track, one is interested in the roles of particles emitted directly from the stack and of the vapors emitted with them. To address this

clean marine case, where the effective radius dropped from 10.8 μm to 3.4 μm in track.

5. Microphysical Processes

Using case studies from section 4 as a basis, we can study the contributions from individual aerosol processes in ship tracks by comparing predicted and observed microphysical features. To study the role of gas-to-particle conversion, we compare droplets activated with and without additional condensable vapor sources provided by SO_2 in the stack effluent. Enhanced particle growth and increased soluble fraction from the condensation of sulfate can change the predicted number of CCN and, consequently, the associated ship track features.

Numerical modeling is used here to represent aerosol and cloud microphysical processes in the marine boundary layer. With case study observations to provide a measure of the quality of our representation of the atmosphere, we compare the roles of several microphysical processes in aerosol evolution. The model described in section 3 includes aerosol dynamics and condensation and coagulation in a Lagrangian air parcel. Two sets of case studies described in section 4 provide field observations with a range of track and background aerosol concentrations. To investigate the potential role of precip-
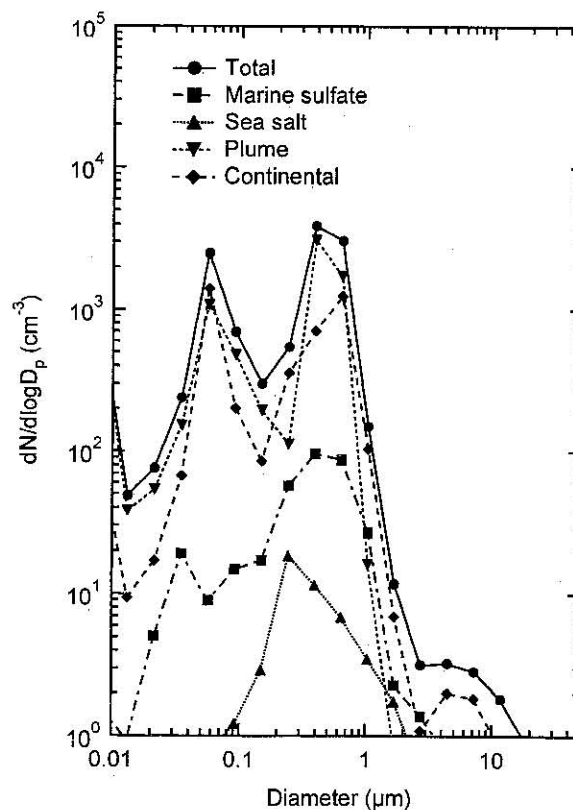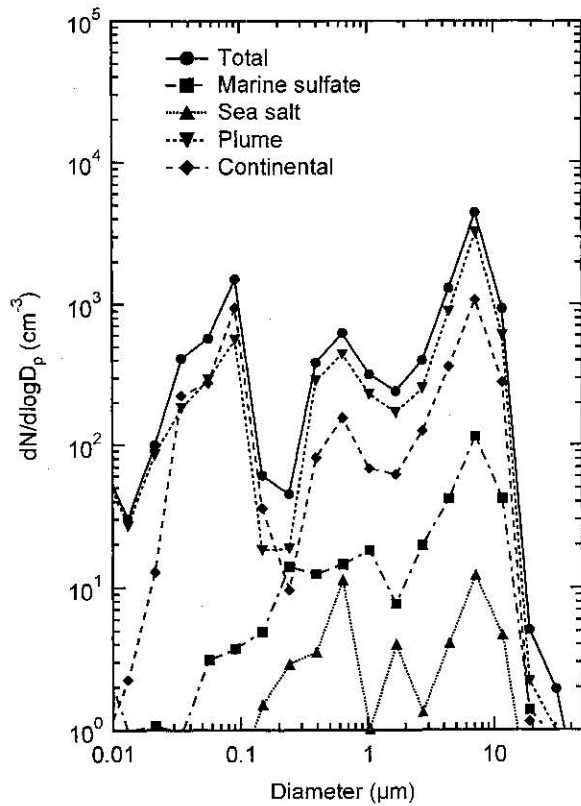

Figure 16. Predicted below-cloud particle size distribution for track air in the continentally- influenced case (JDT 178). Circles show the total aerosol number distribution, squares show marine sulfate particles, triangles show sea salt particles, diamonds show continental particles, and inverted triangles show plume particles.

Figure 17. Predicted in-cloud particle and droplet size distribution for track in the continentally influenced case (JDT 178). Symbol definitions are the same as in Figure 16.

issue we need to know if the particles per se are CCN at typical marine supersaturations; some evidence from observations [Hudson et al., 2000] suggests that many of the plume particles emitted do act as CCN. Hobbs et al. [2000] inferred particle composition from the fraction of particles activated to CCN. Here we take the alternative approach of using data from engine emissions to prescribe compositions for stack-emitted particles. The model prediction that the particles in the track modify the cloud droplet distribution to include more smaller drops in the track is consistent with the prediction from the observed differences in the AVHRR image signatures [Durkee et al., 2000b]. In the clean marine case we would like to determine how much of this signature results from gas-to-particle conversion. By considering the same conditions but restricting gas-to-particle conversion by limiting the stack emissions to be only particles and no sulfur vapors, the resulting distribution of activated droplets is predicted to be significantly less than the predicted track conditions and more similar to the background case.

The results for predicted cloud droplet distributions with no SO_2 in the stack emissions (but with a background SO_2 mixing ratio of 0.34 ppb) are shown in Table 3. This result shows that some of the particles as emitted are not sufficiently efficient CCN to activate at the predicted maximum supersaturation of 0.68%, so that they never effectively compete with the previously existing background particles in taking up liquid water.

Table 3. Predicted Variation of Cloud Characteristics for Track and Background Conditions for the Clean Marine Case (JDT 180) and the Continentally Influenced Case (JDT 178)

	Liquid Water Content (g m^{-3})		Effective Radius (μm)		Droplet Number (cm^{-3})		Maximum Supersaturation	
	Background	Track	Background	Track	Background	Track	Background	Track
Updraft Velocity (w=0.3 m s^{-1})								
w=0.5 m s^{-1} (JDT 180)	+0.04	+0.06	+0.1	-0.6	+3	+1060	+0.23%	+0.04%
w=0.5 m s^{-1} (JDT 178)	+0.07	+0.06	-0.1	-0.4	+91	-40	+0.10%	+0.05%
w=0.2 m s^{-1} (JDT 180)	-0.02	-0.02	-0.2	+0.3	+1	+870	-0.16%	-0.02%
w=0.2 m s^{-1} (JDT 178)	-0.04	-0.05	-0.2	+0.4	+58	-150	-0.05%	-0.04%
Updraft Area Fraction (55%)								
65% (JDT 180)	+0.03	+0.04	0	0	+10	+390	0	0
65% (JDT 178)	+0.04	+0.04	0	0	+55	+179	0	0
45% (JDT 180)	-0.03	-0.04	0	0	-10	-390	0	0
45% (JDT 178)	-0.04	-0.04	0	0	-55	-179	0	0
Dilution (100% Emissions)								
50% emissions (JDT 180)	NA	0	NA	-0.3	NA	+120	NA	+0.04%
50% emissions (JDT 178)	NA	-0.01	NA	+1.0	NA	-710	NA	+0.04%
10% emissions (JDT 180)	NA	0	NA	+2.3	NA	-3270	NA	+0.15%
10% emissions (JDT 178)	NA	0	NA	+1.6	NA	-1142	NA	+0.12%
Gas-to-Particle Conversion (SO_2 and Particles Emitted)								
No emitted SO_2 (JDT 180)	NA	0	NA	+0.2	NA	-2080	NA	+0.22%
No emitted particles (JDT 180)	NA	-0.01	NA	+7.1	NA	-3784	NA	+0.49%

All values refer to the difference from the "Updraft Only" base case value (specified in parentheses for each section) to the value noted for the case given. ("NA" indicates that there is no sensitivity calculated for this set of conditions.)

The predicted cloud has a lower droplet concentration than in the track case, with a droplet concentration of only 1960 cm^{-3}. With a faster updraft of 0.5 m s^{-1} the same no-SO$_2$ case yields a droplet concentration similar to the background cloud. In this case there is even less time for particle growth from the small amount of background SO$_2$ (i.e., 3 min rather than 6 min) and no plume particles grow large enough to be CCN at the maximum supersaturation. This difference from the actual case, which included stack-emitted SO$_2$ vapors, results from the fact that the plume particles at their measured size on emission are both too small and too insoluble (without the addition of sulfate by condensation in and immediately after the stack) to be CCN at lower supersaturations. The size on emission for the *Star Livorno* case is derived from measurements approximately 100 m away from the stack and so is likely to be an overestimate of the actual size on leaving the stack. Their composition of 50% organic and 50% black carbon is based on power plant engines burning heavy fuel [*Hildemann et al.*, 1991], providing a value that is well within the range that can be expected for a ship engine (excluding the sulfate which we account for separately here). We note, however, that there is a large range of possible particle compositions depending not only on exact engine type but also on maintenance history, operating procedures, stack conditions, fuel source, and ship speed [*Gasparovic*, 1995]. Conversely, emitted SO$_2$ is not sufficient to nucleate and grow new CCN before the first cloud cycle. The results of this sensitivity study for the case of no plume particles is shown in Table 3.

Gas-to-particle formation may also be a mechanism influential in the persistence of ship tracks for multiday periods [*Ferek et al.*, 1998]. To address this question, we first discuss the general role of this process illustrated in four case studies analyzed with the aerosol dynamics model.

Ship track formation is defined as the first cycle of the plume particles through cloud in which they are activated and, consequently, change the predicted droplet number and effective radius in track relative to the same cycle in the background cloud. For gas-to-particle conversion to be important in these secondary stages of evolution of the ship track, there has to be a source of condensable vapor present in the air parcel after that first cloud cycle to cause the particles to grow further. In this work we have not employed models capable of simulating large eddies that would allow us to predict the degree to which stack vapors may be mixed in from adjacent parcels that might not have undergone the same cloud cycle. Given this limitation, our predictions show that SO$_2$ is transferred rapidly in the first cloud cycle to activated droplets, in agreement with the observations that concentrations of SO$_2$ in cloud near the beginning of the track are comparable to those in background cloud. As a result of this, gas-to-particle conversion of SO$_2$ to sulfate in droplets by heterogeneous oxidation contributes to growth of those CCN

activated initially but, in the absence of changes in the supersaturation in later cloud cycles, does not suggest a mechanism for growing additional CCN that might be available to replace those particles lost to coalescence and scavenging in cloud.

5.2. Precipitation

The Clermont-Ferrand DESCAM model [*Flossmann et al.*, 1985] calculates cloud dynamics on the basis of an aircraft sounding of the boundary layer structure. The DESCAM model differs from the Princeton model in that it has the ability to consider a nonadiabatic air parcel which explicitly allows entrainment of air. The features and limitations of these models are summarized in Table 4. In addition, the growth of precipitation-sized drops is calculated more accurately by DESCAM, since it contains 69 droplet size classes and the fixed dry-size grid of the Princeton model has limited resolution for drops above 10 μm diameter. The predictions for the clean marine case confirm that simply by changing the input aerosol distribution from the clean background marine air to a plume aerosol from a ship stack, the resulting cloud droplet distribution was shifted to smaller sizes, as is shown in the case studies in section 4 for clean marine conditions. The track simulation also showed much higher droplet concentrations than in the background.

This marine air case involved an anomalously clean background aerosol concentration and so was chosen to study the hypothesis that ship tracks could modify the cloud droplet distribution sufficiently to inhibit precipitation locally. We studied the growth of droplets to determine if they become sufficiently large to form drizzle (approximately 20 μm diameter) during their estimated time in the 220 m thick cloud at an updraft velocity of between 0.5 and 0.3 m s^{-1}. In this case, the time required for growth to droplets by condensation and coalescence mechanisms was longer than the time in the cloud updraft region (approximately 7 to 12 min) in both track and background clouds, suggesting that in order for drizzle to form, longer times within the cloud layer are needed. This result implies that the simple single-parcel dynamics model used here is not sufficient to address drizzle formation and that a LES, which can explicitly allow mixing of parcels and can predict variations in supersaturation in multiple cloud cycles, would be required in order to predict the detailed cloud residence times required for this question.

6. Measurement and Model Uncertainties

Important uncertainties underlie both measurements and model predictions in the atmospheric processes compared here. The effects of several key uncertainties are shown in Table 3. In the MAST experiment, measurements of organic composition and of size-resolved inorganic components were lacking. While these mea-

Table 4. Comparison of Features and Limitations of Princeton and Clermont-Ferrand (DESCAM) Models

Model Features	Princeton	Clermont-Ferrand (DESCAM)
General		
Mechanism studied	gas-to-particle conversion	precipitation
Reference	*Russell and Seinfeld* [1998]	*Flossmann et al.* [1989]
Cases studied	JDT 180 background	JDT 180 background
	JDT 180 track	JDT 180 track
	JDT 178 background	
	JDT 178 track	
Thermodynamic		
Structure	parcel in 1-D grid	parcel
Aerosol		
Size description	40 dry fixed sections, moving section water	81 aerosol sections, 69 droplet sections
Mixtures	external and internal	internal
Vapor-liquid equilibrium	multicomponent nonideal equilibrium	ideal equilibrium
Droplet activation	kinetic rate of activation	instantaneous activation of CCN
Cloud		
Lapse rate	prescribed measured profile	nonadiabatic with entrainment
Updraft velocity	prescribed updraft velocity	prescribed updraft velocity
Microphysics	explicit coagulation and coalescence	explicit coagulation, coalescence, and scavenging
Chemistry		
Homogeneous	sulfur oxidation	none
Heterogeneous	sulfur oxidation	none

surements are feasible with existing technology, they are limited by inlet losses and by long sampling times required to collect sufficient material for off-line analysis [*Huebert et al.*, 1998]. On-line single-particle composition measurements have been achieved for higher-altitude measurements but do not provide quantitative mass composition [*Murphy et al.*, 1998]. Detailed knowledge of the distribution of species among external mixtures of aerosols would nonetheless be valuable in future studies.

An important overprediction by the model compared to the measurements in the track for the clean marine (JDT 180) and continentally influenced (JDT 178) cases occurs in cloud droplet number concentrations and to a lesser extent in liquid water content. This difference results from the simplified parcel scheme in the model as well as instrument and sampling limitations in the measurements. Predicted cloud droplet concentrations exceeding 1000 cm^{-3} cannot persist beyond short updrafts and so comparing such predictions to ambient averages is not possible.

6.1. Limitations on Sampling

Several fundamental parameters in cloud formation cannot be measured with currently available techniques, including updraft velocity and rate of change of supersaturation for the time history of a single parcel or of an aggregate of parcels. Perhaps of greater importance is the limitation that both modeling and sampling in sufficient detail to instantaneously characterize a chemically detailed three-dimensional cloud in time remain technologically challenging, so we still need to infer properties from various constant altitude averages to compare them to the modeled updraft regions of our parcel model. *Feingold et al.* [1998] modeled detailed internally mixed size distributions with 500 air parcel trajectories, providing a spatially resolved (but not fixed) grid in which aerosol evolution could be tracked but without the additional computational burden of externally mixed aerosol. Incorporating an externally mixed aerosol in the *Feingold et al.* [1998] trajectory ensemble model (TEM) would allow one to study the range and standard deviation of the results predicted here as well as longer time evolution questions. The LES approach of *Kogan et al.* [1995] would be required to quantify the mixing of parcels of background air with track aerosol, if a computationally efficient aerosol description can be devised to incorporate track aerosol complexity.

6.2. Effect of Updraft Velocity

Uncertainty in the estimated updraft velocity suggests a range of possible velocities between 0.2 and 0.5 m s^{-1} [*Nicholls and Leighton*, 1986]. The effect of this variation on the predicted cloud formation is shown in
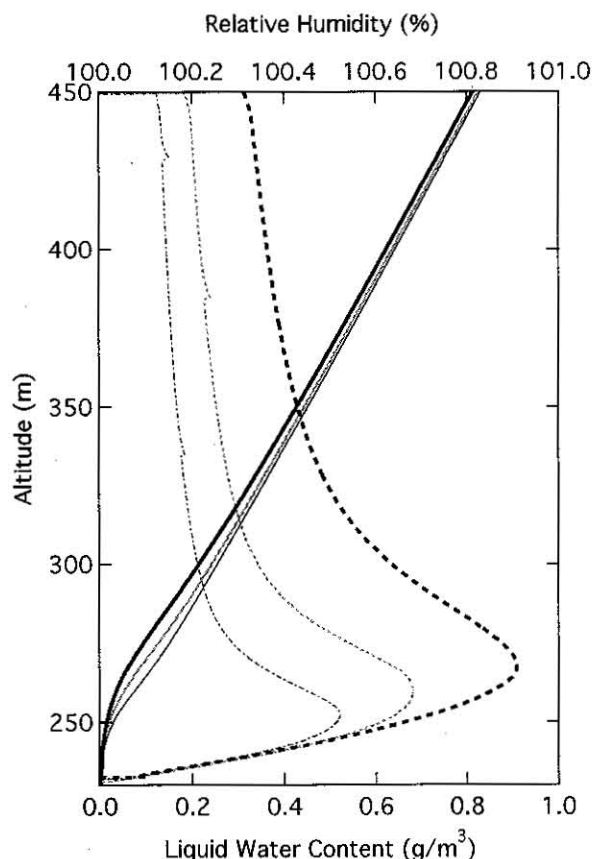
Relative Humidity (%)

Figure 18. As for Figure 7, but for three different updraft velocities. Thin gray solid line shows liquid water content, and thin gray dashed line shows relative humidity in the background for the clean marine case (JDT 180) for the base case updraft velocity of $w = 0.3$ m s^{-1}. The thick solid line shows liquid water content, and the thick dashed line shows relative humidity for the updraft velocity of $w = 0.5$ m s^{-1}. The thin black solid line shows liquid water content, and the thin black dashed line shows relative humidity for the updraft velocity of $w = 0.2$ m s^{-1}.

Figure 18 and is summarized in Table 3. The maximum supersaturation reached with an updraft velocity $w = 0.5$ m s^{-1} is increased to 0.91%, whereas for the slower value of $w = 0.2$ m s^{-1} only 0.42% is predicted. For low concentrations there is a significant impact on the maximum supersaturation reached in cloud, although the small number of very efficient CCN present in this case results in almost no change in cloud droplet number or liquid water content. The track prediction in the clean marine case shows a significant change in droplet number concentration and effective radius at an updraft velocity of $w = 0.5$ m s^{-1} but also shows an increase in cloud droplet number for the updraft velocity of $w = 0.3$ m s^{-1} since there is a longer time available to grow particles by condensation.

6.3. Effect of Updraft Area Fraction

Updraft regions with growing droplets will produce larger droplet distributions and higher average liquid water contents than the downdraft regions with evaporating and subsaturated droplets [*Stevens et al.*, 1996]. We have estimated this effect using an estimated updraft area fraction of 55% in the results in Table 2. The resulting predicted value is expected to represent the measurement better since the aircraft sampled both updraft and downdraft regions in unknown amounts. Incorporating an explicit microphysics model in a LES has been used by *Kogan et al.* [1995] to study the fine-scale spatial structure of cloud properties using an internally mixed size-resolved aerosol, but in the absence of this detail, we have estimated the sensitivity of cloud characteristics to variations in the area fraction that covers updrafts. While the maximum supersaturation and effective radius of droplets are essentially unchanged by this parameter, the liquid water content and droplet number vary almost linearly. For instance, with an updraft fraction of 65% the cloud average liquid water content of both the background and the track conditions for the clean marine case (JDT 180) increase to 0.23 g m^{-3} and 0.24 g m^{-3}, respectively, which are both within the standard deviations measured for the background (0.28 g m^{-3} with a standard deviation of 0.05 g m^{-3}) and the track (0.31 g m^{-3} with a standard deviation of 0.11 g m^{-3}).

6.4. Effect of Plume Dilution

Another consequence of the one-dimensional approach that we have employed here is that the rate of dilution was not modeled explicitly and relied on estimates that were insufficiently constrained by the observations. The absence of explicit dilution of the measured initial size distributions may account for much of the overprediction observed in cloud droplet number concentrations in the track conditions. Given the uncertainty of both the peak supersaturation and the degree of dilution, however, there were insufficient measurements to independently constrain these two parameters. To quantify the potential effect of this uncertainty, we have studied the impact of dilution of the plume to 50% and 10% of its emitted particle and SO$_2$ concentrations. In the clean marine case with only 10% of emissions (corresponding to an emitted particle concentration of 1830 cm^{-3}) the maximum supersaturation is 0.33%, which is an increase of 0.15% over the undiluted track but still a significant drop from the background value (0.68%). The updraft cloud droplet concentration also decreases significantly to only 650 cm^{-3}, corresponding to an average cloud droplet concentration of 410 cm^{-3}, but the liquid water content is unchanged.

Since the in-track measurements of cloud droplet concentrations shown in Figures 4 and 12 were sampled at points in the tracks between 1 hour and 2.5 hours after emission, the plume concentrations are estimated to have been dispersed to between 50% and 10% of their original values [*Durkee et al.*, 2000c]. The magnitude of the dilution was not well-defined by the measurements, but these calculations show that the uncertainty in the

degree of dilution is sufficient to account for much of the discrepancy between measured and predicted cloud characteristics.

7. Aerosol Processes in Ship Tracks

Aerosol particles provide additional CCN that activate in ship tracks resulting in enhanced droplet concentrations and decreased mean drop size [*Durkee et al.*, 2000b]. Multiple processes contribute to the characteristics of these CCN, from the point of their formation from vapors in the combustion process and subsequent emission from the ship stack to the atmosphere. Condensation and coagulation contribute to the growth of some particles and the removal of others. Aerosol growth by either condensation or coagulation has the effect of adding water-soluble mass to emitted aerosol nuclei that makes them efficient as CCN at the effective supersaturations expected for marine stratocumulus. Condensation of H_2SO_4 from gas-phase oxidation of SO_2 is primarily responsible for adding soluble sulfate mass to the newly emitted black and organic carbon particles. Once these particles are activated, additional contributions from the aqueous oxidation of SO_2 on activated droplets also grow particles. Some activated and some interstitial aerosol particles are lost by coagulational processes in cloud, resulting in a shift in the size spectrum to larger particles. Whether there is enough residence time for particles in this type of cloud cycle for particles to grow sufficiently large by both condensation and coagulation to precipitate determines whether ship tracks will have feedback effects on both rain and boundary layer structure.

With the exception of the limited information on chemical composition the above uncertainties primarily interfere with our ability to predict the evolution of ship tracks rather than their initial formation. While we have initial evidence that gas-to-particle conversion is not likely to control the evolution of ship tracks after formation due to removal of the bulk of condensable species in the first cloud cycle, uncertainties in oxidant concentrations as well as in thermodynamic profiles of subsequent cloud cycles make this conclusion tentative until additional measurements and modeling is performed.

Gas-to-particle conversion of SO_2 is necessary for ship track formation in the clean marine case studied here. It is not clear how much of this conversion occurs before emission from the stack and how much occurs after emission due to the sampling constraints on particle composition and the lack of detailed, direct stack measurements of emissions. However, without any contribution from sulfate, the insoluble nature of both black carbon and of the slightly soluble organic carbon fraction dictates that the plume particles are too small and too nonhygroscopic to serve as CCN for the maximum supersaturations of from 0.15% to 0.68% predicted for clouds sampled in the MAST experiment. This conclu-

sion suggests that the sulfur composition of fuels used in combustion processes has a direct impact on the indirect effect of these emitted particles on clouds. Further work is needed to determine if nitrogen oxides or organic species would replace the role of sulfur oxides in the event that fuel sulfur were reduced.

References

Bates, T.S., R.J. Charlson, and R.H. Gammon, Evidence for the climatic role of marine biogenic sulfur, *Nature, 329*, 319-321, 1987.

Bates, T.S., J.E. Johnson, P.K. Quinn, P.D. Goldan, W.C. Kuster, D.C. Covert, and C.J. Hahn, The biogeochemical sulfur cycle in the marine boundary layer over the Northeast Pacific Ocean, *J. Atmos. Chem., 10*, 59-81, 1990.

Bott, A., A positive definite advection scheme obtained by nonlinear renormalization of the advective fluxes, *Mon. Weather Rev., 117*, 1006-1015, 1989.

de Bruyn, W.J., T.S. Bates, J.M. Cainey, and E.S. Saltzman, Shipboard measurements of dimethyl sulfide and SO_2 southwest of Tasmania during the First Aerosol Characterization Experiment (ACE 1), *J. Geophys. Res., 103*, 16703-16711, 1998.

Dhaniyala, S., and A.S. Wexler, Numerical schemes to model condensation and evaporation of aerosols, *Atmos. Environ., 30*, 919-928, 1996.

Durkee, P.A., K.J. Noone, and R.T. Bluth, The Monterey Area Ship Track (MAST) experiment, *J. Atmos. Sci.,* in press, 2000a.

Durkee, P.A., et al., The impact of ship produced aerosols on the microphysical characteristics of warm stratocumulus clouds: A test of hypotheses 1.1a and 1.1b, *J. Atmos. Sci.,* in press, 2000b.

Durkee, P.A., R.E. Chartier, A. Brown, E.J. Trehubenko, S.D. Rogerson, C. Skupniewicz, K.E. Nielsen, S. Platnick, and M.D. King, Composite ship track characteristics, *J. Atmos. Sci.,* in press, 2000c.

Erlick, C., L.M. Russell, and V. Ramaswamy, A microphysics-based investigation of the radiative effects of aerosol-cloud interactions for two MAST Experiment case studies, *J. Geophys. Res.,* in press, 2000.

Feingold, G., S.M. Kreidenweis, and Y. Zhang, Stratocumulus processing of gases and cloud condensation nuclei, *J. Geophys. Res., 103*, 19,527-19,542, 1998.

Ferek, R.J., D.A. Hegg, P.V. Hobbs, P.A. Durkee, and K.E. Nielsen, Measurements of ship-induced tracks in clouds off the Washington coast, *J. Geophys. Res., 103*, 23,199-23,206, 1998.

Flossmann, A.I., W.D. Hall, and H.R. Pruppacher, A theoretical study of the wet removal of atmospheric pollutants,

part I, The redistribution of aerosol particles captured through nucleation and impaction scavenging by growing cloud drops, *J. Atmos. Sci.*, *42*, 582-606, 1985.

Gasparovic, R.F., *MAST Experiment Operations Summary*, Johns Hopkins Univ., Maryland, 1995.

Hildemann, L.M., G.R. Markowski and G.R. Cass, Chemical Composition of Emissions from Urban sources of fine organic aerosol, *Environ. Sci. Technol.*, *25*, 744-759, 1991.

Hobbs, P.V., et al., Emissions from ships with respect to their effects on clouds, *J. Atmos. Sci.*, in press, 2000.

Hoppel, W.A., J.W. Fitzgerald, G.M. Frick, and R.E. Larson, Aerosol size distributions and optical properties found in the marine boundary layer over the Atlantic Ocean, *J. Geophys. Res.*, *95*, 3559-3886, 1990.

Hudson, J.G., T.J. Garrett, P.V. Hobbs, S.R. Strader, Y. Xie, and S.S. Yum, Cloud condensation nuclei and ship track clouds, *J. Atmos. Sci.*, in press, 2000.

Huebert, B.J., S.G. Howell, L. Zhuang, J.A. Heath, M.R. Litchy, D.J. Wylie, J.L. Kreidler-Moss, S. Cöppicus, and J.E. Pfeiffer, Filter and impactor measurements of anions and cations during the First Aerosol Characterization Experiment (ACE 1), *J. Geophys. Res.*, *103*, 16,493-16,509, 1998.

Jacobson, M.Z., Numerical techniques to solve condensational and dissolutional growth equations when growth is coupled to reversible reactions, *Aerosol Sci. Technol.*, *4*, 491-498, 1997.

Jacobson, M.Z., R.P. Turco, E.J. Jensen, and O.B. Toon, Modeling coagulation among particles of different composition and size, *Atmos. Environ.*, *28*, 1327-1328, 1994.

Jennings, S.G., and C.D. O'Dowd, Volatility of aerosol at Mace Head, on the west-coast of Ireland, *J. Geophys. Res.*, *95*, 13,937-13,948, 1990.

Kaufman, Y.J., and D. Tanré, Effect of variations in supersaturation on the formation of cloud condensation nuclei, *Nature*, *369*, 45-48, 1994.

Kogan, Y.L., M.P. Khairoutdinov, D.K. Lilly, Z.N. Kogan, and Q. Liu, Modeling of stratocumulus cloud layers in a large eddy simulation model with explicit microphysics, *J. Atmos. Sci.*, *52*, 2923-2940, 1995.

Kulmala, M., and A. Laaksonen, Binary nucleation of water-sulfuric acid system: Comparison of classical theories with different H_2SO_4 saturation vapor pressures, *J. Chem. Phys.*, *93*, 696-701, 1990.

de Laat, A.T.J., and P.G. Duynkerke, Analysis of ASTEX-stratocumulus observational data using a mass-flux approach, *Boundary Layer Meteorol.*, *86*, 63-87, 1998.

Murphy, D.M., D.S. Thomson, A.M. Middlebrook, and M.E. Schein, In situ single-particle characterization at Cape Grim, *J. Geophys. Res.*, *105*, 16,485-16,491, 1998.

Nicholls, S., and J. Leighton, An observational study of the structure of stratiform cloud sheets, part I, Structure, *Q. J. R. Meteorol. Soc.*, *112*, 431-460, 1986.

Noone, K.J., et al., A case study of ship track formation in a polluted boundary layer, *J. Atmos. Sci.*, in press, 2000a.

Noone, K.J., et al., A case study of ships forming and not forming tracks in a moderately polluted boundary layer, *J. Atmos. Sci.*, in press, 2000b.

Pandis, S.N., L.M. Russell, and J.H. Seinfeld, The relationship between DMS flux and CCN concentration in remote marine regions, *J. Geophys. Res.*, *99*, 16945-16958, 1994.

Quinn, P.K., T.S. Bates, J.E. Johnson, D.S. Covert, and R.J. Charlson, Interactions between the sulfur and reduced nitrogen cycles over the Central Pacific Ocean, *J. Geophys. Res.*, *95*, 16,405-16,416, 1990.

Richards, L.W., J.A. Anderson, D.L. Blumenthal, J.A. McDonald, G.L. Kok, and A.L. Lazrus, Hydrogen peroxide and sulfur (IV) in Los Angeles cloud water, *Atmos. Environ.*, *17*, 911-914, 1983.

Russell, L.M., and J.H. Seinfeld, Size- and composition-resolved externally- mixed aerosol model, *Aerosol Sci. Technol.*, *28*, 403-416, 1998.

Russell, L.M., S.N. Pandis, and J.H. Seinfeld, Aerosol production and growth in the marine boundary layer, *J. Geophys. Res.*, *99*, 20,989-21,003, 1994.

Russell, L.M., R.C. Flagan, and J.H. Seinfeld, Asymmetric instrument response due to mixing effects in DMA-CPC measurements, *Aerosol Sci. Technol.*, *23*, 491-509, 1995.

Russell, L.M., M.R. Stolzenburg, S.H. Zhang, R. Caldow, R.C. Flagan, and J.H. Seinfeld, Radially-classified aerosol detector for aircraft-based submicron aerosol measurements. *J. Atmos. Oceanic Technol.*, *13*, 598-609, 1996.

Seinfeld, J.H., and S.N. Pandis, *Atmospheric Chemistry and Physics*, John Wiley, New York, 1998.

Stevens, B., G. Feingold, W.R. Cotton, and R.L. Walko, Elements of the microphysical structure of numerically simulated nonprecipitating stratocumulus, *J. Atmos. Sci.*, *53*, 980-1006, 1996.

Tzivion, S., G. Feingold, and Z. Levin, An efficient numerical solution to the stochastic collection equation, *J. Atmos. Sci.*, *44*, 3139-3149, 1987.

Weber, R.J., P.H. McMurry, F.L. Eisele, and D.J. Tanner, Measurement of expected nucleation precursor species and 3-500-nm diameter particles at Mauna Loa Observatory, Hawaii, *J. Atmos. Sci.*, *52*, 2242-2257, 1995.

Wexler, A.S., and J.H. Seinfeld, The distribution of ammnium salts among a size and composition dispersed aerosol, *Atmos. Environ.*, *24(A)*, 1231- 1246, 1990.

L.M. Russell, Department of Chemical Engineering, A317 Engineering Quadrangle, Princeton University, Princeton, NJ 08544. (lrussell@princeton.edu)

R.C. Flagan and J.H. Seinfeld, Department of Chemical Engineering, California Institute of Technology, Pasadena, CA 91125. (flagan@cco.caltech.edu, seinfeld@cco.caltech.edu)

R.J. Ferek, Office of Naval Research, 800 N. Quincy St., Arlington, VA 22217. (ferekr@onr.navy.mil)

D.A. Hegg and P.V. Hobbs, Department of Atmospheric Sciences, University of Washington, Seattle, WA 981950. (deanhegg@atmos.washington.edu; phobbs@atmos.washington.edu)

P.A. Durkee and K.E. Nielsen, Department of Meteorology, Code MR/De, Naval Postgraduate School, 589 Dyer Rd., Rm. 254, Monterey, CA 93943. (durkee@nps.navy.mil, kenielsen@ nps.navy.mil)

A.I. Flossmann and W. Wobrock, Universite Clermont-Ferrand, Laboratoire Meteorologie Physique, CNRS, 24 Ave. Landais, Clermont-Ferrand F-63177 Aubiere, France. (flossman@opgc.univ-bpclermont.fr)

C.D. O'Dowd, University of Sunderland, School of the Environment, Center for Marine and Atmopsheric Sciences, Benedict Bldg., St. Georges Way, Sunderland SR2 7BW, Durham, England. (colin.odowd@cmas.demon.co.uk)